

## Effects of Process Induced Differences in Power Bed Feedstock Particle Size Distribution for Processability and Quality In PBF-LB/M

N. A. Pielczyk\*, J. Mireles\*, and R. B. Wicker\*

\*W.M. Keck Center for 3D Innovation, University of Texas at El Paso, El Paso, TX 79968

### Abstract

Particle size distribution (PSD) variations significantly impact the processability and performance of parts manufactured through Laser Powder Bed Fusion (LPBF). This study investigates the effects of PSD on IN718 powder using a comprehensive experimental approach that addresses realistic manufacturing scenarios. Through single-layer and multi-layer experiments, the research systematically examined how PSD differences influence melt pool geometry, surface roughness, and mechanical properties. In the single-layer experiment, finer powder demonstrated a more stable process window and distinct melt pool characteristics. Surface roughness measurements revealed significantly higher values for finer powder, with a one-way ANOVA confirming statistically significant. The depth-to-height (D/H) ratio analysis showed that finer powder resulted in more consistent melt pool geometry across various energy densities. The multi-layer experiment unveiled notable hardness variations between powders with different particle size distributions. Vickers hardness (HV0.1) measurements indicated that the finer powder exhibited approximately 6.8 % higher hardness compared to coarser powder, with statistical significance confirmed through ANOVA testing. Preliminary microstructural analysis suggested potential microstructural differences correlating with particle size distribution. These findings underscore the critical importance of understanding and managing particle size distribution in additive manufacturing. The research provides insights into how PSD variations can impact process stability, surface characteristics, and mechanical properties, highlighting the need for precise powder characterization and potential process parameter adjustments in LPBF manufacturing.

### Introduction

Additive manufacturing using Laser Powder Bed Fusion (AM-LPBF) has seen significant advancements in recent years, driven by its capability to produce complex geometries and high-performance components [1, 2]. However, process consistency and part quality remain critical challenges [1, 2, 3, 4, 5, 6, 7]. Previous research conducted at the W.M. Keck Center for 3D Innovation has indicated that differences in particle size distribution (PSD) substantially affect the emissivity and absorptivity behavior of powders, as described by the gray-body theorem [8, 9]. For instance, previous investigations revealed that PSD variations achieved solely by spreading powder across the substrate plate or powder bed resulted in a notable 6.4% increase in absorptivity for finer powders compared to coarser powders. Despite these findings, there is a lack of comprehensive investigations into realistic PSD differences encountered during actual AM-LPBF operations and their potential impacts on processability and the quality of finished parts. Existing studies primarily focus on controlled PSD differences that are unlikely to occur in typical manufacturing scenarios [10, 11, 12, 13]. For example, refinements in PSD have been shown to significantly affect the process parameter window, defined by the fundamental volumetric energy density  $E_v$  [ $J/mm^3$ ] (equation 1), particularly in terms of scanning speed ( $v_s$  [mm/s]) and laser power ( $P_l$  [W]) [14, 15, 16]. Finer powders exhibit broader parameter combinations that produce fully dense parts, while coarser powders are more prone to defects such as porosity or lack of fusion (LOF) [13, 17, 18]. However, these investigations typically involve PSDs with median particle sizes ( $D_{50}$  [ $\mu m$ ]) ranging from 16  $\mu m$  to 76  $\mu m$ , which are not representative of real-world conditions [10].

$$E_v = \frac{P_l}{v_s * h_s * l_z} \left[ \frac{J}{mm^3} \right] \quad (1)$$

In terms of mechanical properties, several studies have shown that PSD refinement enhances the yield strength (YS) and ultimate tensile strength (UTS) of components, with increases ranging from 12–57 % and 10–30 %, respectively, in IN718 feedstock [19, 20]. However, this improvement often comes at the expense of reduced elongation ( $\epsilon$  [%]) [20]. While the influence of particle shape, such as the improved regularity of plasma-atomized powders compared to gas-atomized powders, has been extensively studied, the isolated effects of PSD refinement on fatigue performance remains largely unexplored. General trends identified concerning hardness (Rockwell, Vickers) and toughness (Charpy) testing indicate increase property values for refined powder, however, investigated PSD differences are not representative for actual in-process occurrence [18, 21, 22].

Recognizing the importance of PSD in LPBF processes could significantly enhance manufacturing efficiency by reducing part rejection rates during quality assurance testing. Moreover, it could improve the viability of powder reuse strategies, which are crucial for cost and resource efficiency. Current reuse methodologies, such as "Top-Up," "Single Batch Method," and "Collective Aging Method," do not account for PSD adjustments, even though sieving and combining powders often lead to PSD changes [3, 23, 24, 25]. Developing an awareness of the need for process parameter adjustments based on PSD conditions is essential for achieving consistent manufacturing quality [3]. This work seeks to bridge the knowledge gap by characterizing the impact of PSD on both processability and part quality. A time- and resource-efficient experimental setup is proposed to enable systematic investigations of PSD effects. Additionally, a real-world case study is presented, focusing on medium-volume production scenarios where:

- Several parts are produced in each job across a substrate plate
- The required powder volume exceeds the capacity of a single powder lot
- Variations arise due to displacement between powder suppliers or recoaters

The hypothesis underpinning this study is that PSD differences in such scenarios cause significant changes in processability, particularly in melt pool geometry, and negatively affect part performance, such as hardness. These variations ultimately hinder the consistent quality required for high-performance applications in AM-LPBF.

## **Materials and Methods**

This study investigates the influence of particle size distribution (PSD) variations on the processability and quality of parts produced through Laser Powder Bed Fusion (LPBF). Prior research has highlighted the significant differences in absorptivity between fine and coarse powders, emphasizing the necessity of understanding these effects on manufacturing outcomes. Plasma-atomized IN718 powder supplied by 3DSystems (Rock Hill, USA) was utilized. PSD was characterized using dynamic image analysis (DIA) on a Camsizer X2 system by Microtrac/Retsch, adhering to ASTM B822-20 standards. Volume-based characteristics were derived in accordance with ASTM E1617-09, focusing on diameter descriptors  $D_{10}$ ,  $D_{50}$ , and  $D_{90}$ . The minimal particle size,  $x_{\text{cmin}}$  [ $\mu\text{m}$ ], was measured following ASTM E11-22 guidelines. Three independent measurements of 20 g samples were performed to ensure statistical robustness, with calibrated feeder settings providing repeatability. Sampling adhered to ASTM B215-20, with a randomized container selection process executed via an RStudio script to ensure unbiased results.

Two lots from the same powder batch were analyzed, and deviations between lots were attributed to powder segregation and atomization process parameters, such as dispersion and atomization pressure differences. These findings are elaborated in Chapter 1. Previous investigations indicate that displacement-fed recoaters, such as those in the ACONITY MIDI+ system, cause PSD gradients across the substrate plate, with significant variation along the recoater's travel direction. This phenomenon, combined with absorptivity differences (finer powder showing a 6.4 % higher absorptivity than coarser powder), necessitates a comprehensive "worst-case scenario" analysis.

Characteristic	Lot		$\Delta$ [%]
	20MP01261C	490655	
D <sub>10</sub> [ $\mu\text{m}$ ]	21.5	24.6	12.7
D <sub>50</sub> [ $\mu\text{m}$ ]	33.7	35.0	3.6
D <sub>90</sub> [ $\mu\text{m}$ ]	46.3	48.1	3.7

Table 1: D-Characteristics Data Comparison – Lot Dependency

Characteristic	Sampling location		$\Delta$ [%]
	First contact	Last contact	
D <sub>10</sub> [ $\mu\text{m}$ ]	19.0	21.7	12.4
D <sub>50</sub> [ $\mu\text{m}$ ]	29.7	33.3	10.9
D <sub>90</sub> [ $\mu\text{m}$ ]	43.2	46.0	6.1

Table 2: D-Characteristics Data Comparison – Sampling Location Dependency

Characteristic	Powder identifier		$\Delta$ [%]
	Superpos1 / Sample1	Superpos2 / Sample2	
D <sub>10</sub> [ $\mu\text{m}$ ]	22.6	16.6	26.5
D <sub>50</sub> [ $\mu\text{m}$ ]	34.5	28.2	18.3
D <sub>90</sub> [ $\mu\text{m}$ ]	45.9	31.0	10.7

Table 3: D-Characteristics Data Comparison – “worst case scenario” superposition

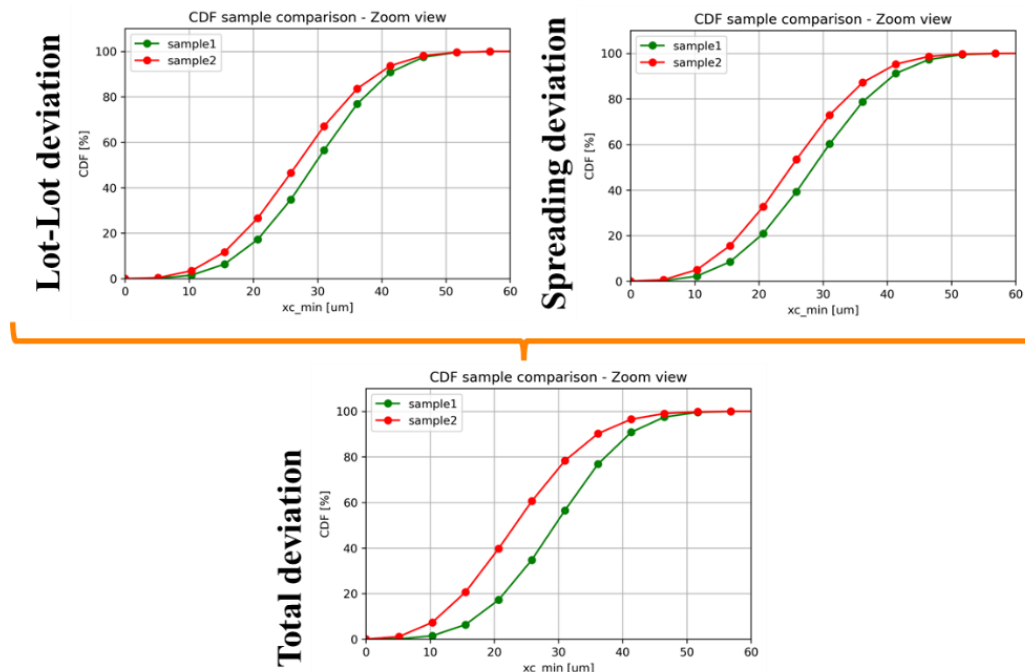


Figure 1: Superposition of Deviation Phenomena

Software developed at the W.M. Keck Center for 3D Innovation facilitated the creation of PSD blends to simulate this scenario, achieving over 98 % repeatability between simulation and actual powder blends. Blends were prepared using a chute splitter (ASTM B215-20) and verified with the Camsizer X2. The graphical results of the cumulative distribution functions are depicted in Figure 1, with the numerical diameter lot-to-lot deviations presented in Table 1, spreading deviations in Table 2, and the superimposed total deviations in Table 3. These configurations served as the basis for subsequent experimental comparisons and analytical/statistical evaluations.

Experiments were conducted using an adjusted ACONITY MIDI+ system (Aconity3D GmbH, Herzogenrath, Germany), optimized for resource efficiency and isolation of variables. A reduction adapter for the substrate plate enabled the use of a smaller 1" x 1" IN718 scan plate, significantly reducing material requirements. A custom gravity-fed recoater, designed and manufactured at the W.M. Keck Center, was mounted on the OEM recoater arm. The recoater utilized a carbon fiber brush trimmed for the reduced substrate dimensions. Parts required for the experimental setup were manufactured at W.M. Keck Center for 3D Innovation utilizing a Stratasys Neo450 VAT polymerization system processing the WaterShed XC11122 material. The supplier system, equipped with eight chambers, dispensed powder incrementally through a chute splitter. Each chamber was filled with 3 g of powder, ensuring consistent layer deposition. A cross-sectional representation of the experimental setup is depicted in Figure 2. The recoater's start and end points were precisely aligned using ACONITY STUDIO's user-friendly controls, ensuring homogeneity across the reduced substrate geometry during the recoating process and consistent repeatability of the process. The general experimental procedures adhered to the listed LPBF conditions:

Powder layer thickness	60 $\mu\text{m}$
Recoating speed	50 mm/s
Oxygen Level	<10000 ppm
Argon inert gas atmosphere	
Scan vectors aligned / parallel with gas flow	

Table 4: General Process Parameter Setup

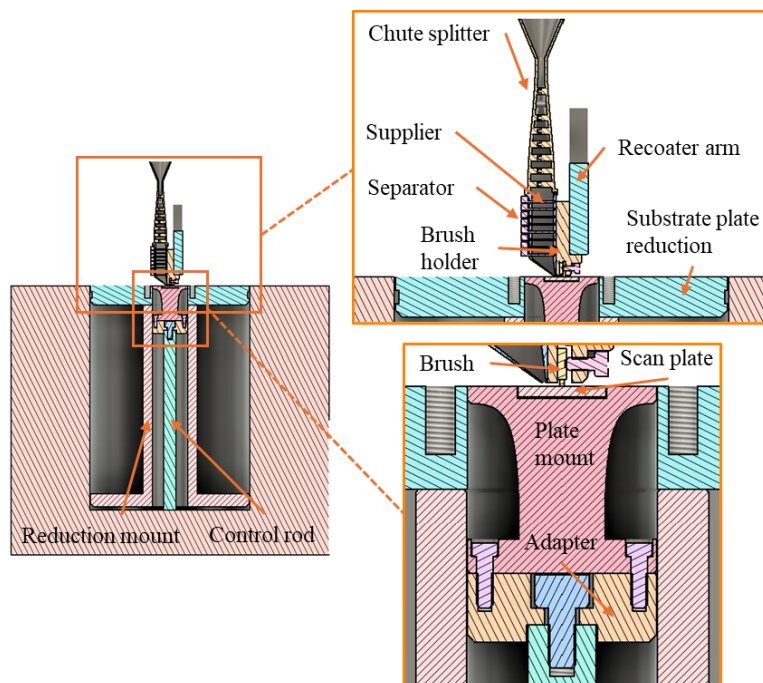


Figure 2: Experimental ACONITY MIDI+ Setup

**Single-Layer Experiment:** The primary objective of the single-layer experiment is to investigate the impact of particle size distribution (PSD) variations on the processability of the powder material in the Laser Powder Bed Fusion (LPBF) process. The study focuses on assessing how these variations influence the geometry of the melt pool, surface roughness, and the overall consistency of the melt pool during the manufacturing process. Previous experiments conducted at the W.M. Keck Center for 3D Innovation, as well as trends observed in literature, indicate that differences in absorptivity between fine and coarse powders can significantly affect processability, which ultimately impacts the quality of the final parts.

A total of 21 parameter variations, based on the parameter ranges presented in Table 5, were selected to evaluate the influence of PSD variations on processability. These variations are designed to impact the line energy density ( $E_l$  [J/mm]), Equation 2. The objective was to determine whether the PSD variation, specifically between Superpos1 and Superpos2, has an effect on the processability of the material. The impact of these variations was evaluated by observing changes in melt pool geometry, particularly the depth and height of the melt pool. For each experimental parameter combination, a single scan track was made on the scan plate. The scan parameters included a track/hatch distance of 1 mm and a scan length of 20 mm. The parameter combinations were randomly assigned a specific track/hatch, as depicted in Figure 3, utilizing an customized Python script for randomization.

Factor	Initial	Level
$P_l$ [W]	280	150, 200, 250, 300, 350
$v_s$ [mm/s]	1000	600, 800, 1000, 1200

Table 5: Single Layer Experiment Factor Levels

$$E_l = \frac{P_l}{v_s} \left[ \frac{J}{mm} \right] \quad (2)$$

To ensure proper alignment and avoid displacement of the scan plate during recoating, the scan plate was mounted into a socket using modeling clay as an adhesive. This also facilitated achieving a level, smooth surface with respect to the top surface of the scan plate, its mount, and the substrate plate reduction.

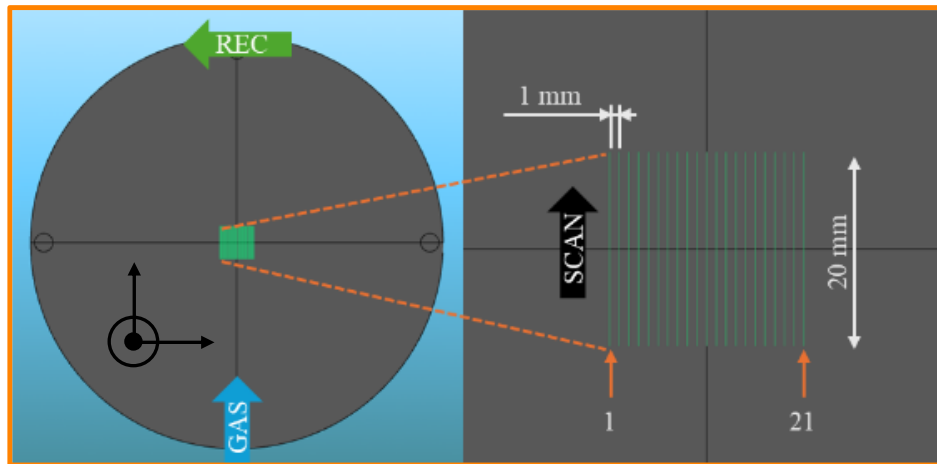


Figure 3: Single-Layer Setup

The line-surface roughness of the scan tracks was measured using the KEYENCE VHX-5000 digital optical microscope. Surface roughness ( $R_a$  [ $\mu\text{m}$ ]) was measured along the symmetry line of each scan track. The lateral tilt of the scan track surface was compensated for during the measurement process to ensure accurate results. The roughness was calculated based on the following equation, whereas  $l$  [ $\mu\text{m}$ ] is the measurement length and  $z(x)$  [ $\mu\text{m}$ ] is the height of individual measurement data points above the measurement's reference surface:

$$R_a = \frac{1}{l} \int_0^l |z(x)| dx \quad [\mu\text{m}] \quad (3)$$

Additionally, melt pool measurements were taken using the KEYENCE VHX-7000 digital optical microscope. The dimensions measured included melt pool depth (D [ $\mu\text{m}$ ]) and melt pool height (H [ $\mu\text{m}$ ]) relative to the surface level of the scan plate. These cross sectional measurements were conducted after the scan plate was sectioned, ground, and polished using Kallings No. 2 etchant to prepare the surface for analysis. The measurement methods for both surface roughness and melt pool geometry are schematically illustrated in Figure 4. The left illustration presents the surface roughness measurements along three scan tracks, while the illustrations on the right side depict the melt pool depth and height measurements for a single scan track.

Prior to the main experiments, a scouting experiment was conducted to assess the potential correlation between aspect ratios and PSD variations. Based on the preliminary results, no significant dependency or correlation was observed between aspect ratios and PSD<sup>1</sup>. This finding led to the conclusion that while aspect ratios may not show a direct link to PSD, the melt pool geometry and surface roughness are more sensitive to changes in PSD.

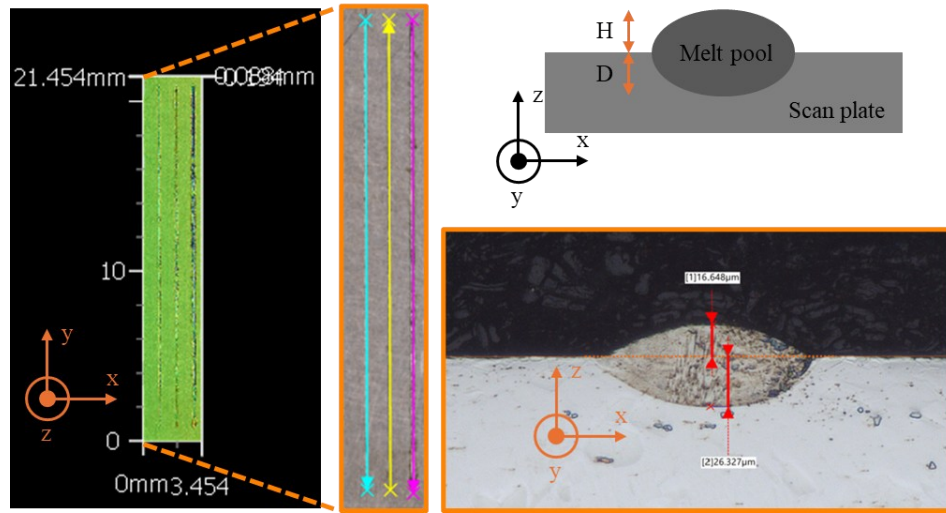


Figure 4: Melt Pool Measurements

**Multi-Layer Experiment:** The multi-layer experiment aims to evaluate the influence of different powder compositions on the properties of laser powder bed fusion (LPBF) parts while maintaining as many process and environmental variables as possible. To minimize variables, the comparison of powders is conducted within the same multi-layer specimen, meaning the machine will not be opened to change the material during the experiment. Instead, the powder is loaded into four chambers, with one chamber containing the first powder type and the remaining chambers containing the second powder type. To address the heat-related issue of mounting the scan plate with modeling clay (which softens and causes displacement during recoating), a different approach was implemented. Instead of using modeling clay, the powder is compressed into the voids between the scan plate and its mount. This allows for the alignment of the scan plate's surface, although it may not be perfectly aligned. To improve the alignment, a sacrificial layer is used, consisting of the same type of powder as the one in the chamber that is being opened first. Approximately 5 g of powder is manually placed in front of the recoater to create the sacrificial layer, which helps level the scan plate's surface for the actual powder layers that will form the multi-layer specimen. Powder loading of the supplier chambers follows two specific sequences:

<sup>1</sup> Measurement data and statistical evaluation available upon request

- Superpos12: 5 layers of Superpos1 powder followed by 4 layers of Superpos2 powder
- Superpos21: 5 layers of Superpos2 powder followed by 4 layers of Superpos1 powder

This inversion of the sequence is done to ensure that the initial contact with the scan plate, as well as the sequence of powder layers, does not affect the process or the final quality of the specimen. The process parameters and exposure strategy applied for the multi-layer experiment, the specimen manufacturing, are presented in Table 6 below.

Laser power	280 W
Scan speed	1000 mm/s
Recoater speed	50 mm/s
Layer thickness	60 $\mu\text{m}$
No scan vector rotation – unidirectional scanning	
Initial scan location	Indicated by a red dot
Scan region	20 mm x 20 mm

Table 6: Process Parameters / Setup

After the multi-layer specimen is manufactured, it is sectioned at the center to provide a cross-sectional (z-x) view of the melt pools and the overall multi-layer structure as schematically depicted in Figure 5. This cross-section is then prepared for further analysis by grinding, etching, and polishing. The etching process is carried out using Kallings No. 2 etchant. Hardness testing is performed on the specimen according to ASTM E92-17 guidelines, specifically using the Vickers hardness test with an applied load of HV0.1. The hardness measurements are conducted using the QNESS 30 CHD Master+ from QATM. For each series of measurements, 10 indentations are made in the same powder region of the specimen. These measurements are repeated across several runs, alternating between regions of the specimen with different powder compositions. If necessary, the indentations are manually checked and remeasured to ensure accurate hardness calculations in compliance with ASTM guidelines.

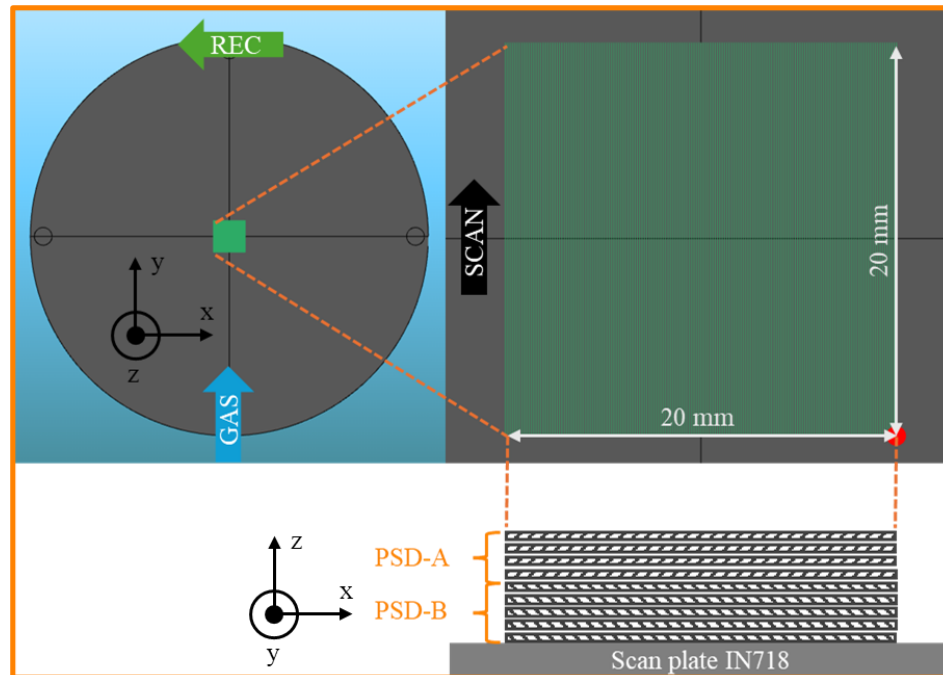
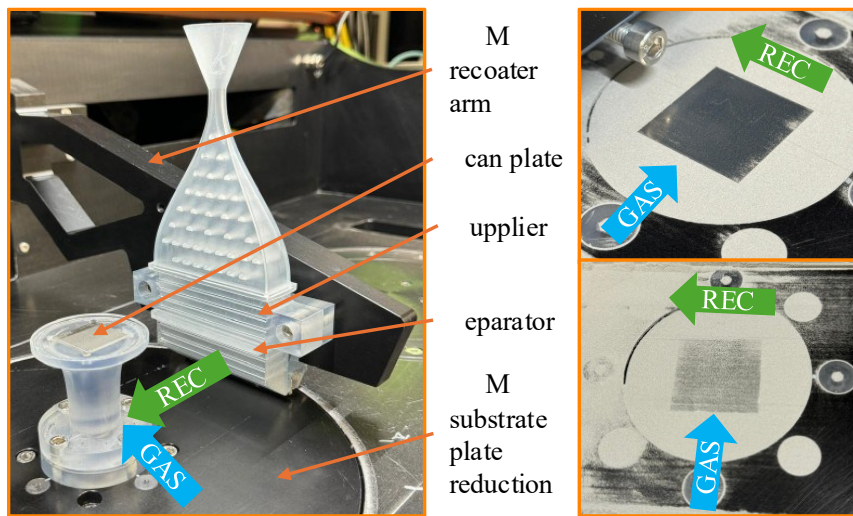


Figure 5: Multi-Layer Setup

## Results and Discussion

The setup developed, manufactured, and tested as described in Chapter 2, and illustrated in Figure 3 and Figure 6, successfully enables consistent and homogeneous powder application on the scan plate. The top right corner image shows the fully prepared scan plate setup. A fraction of the prepared powder for the actual experiment is utilized to establish a level and plane recoating region surrounding the scan plate. The powder is manually placed in front of the recoater brush which then distributes the powder across the scan plate and its mount. The displacement rod connected to the mount and hence the scan plate is repositioned that no residual powder is covering the scan plate ensuring that the subsequent single layer is recoated with the desired layer thickness. Residual powder on the scan plate's edges is blown off by using a handheld air pump. The bottom right image presents the single powder layer after recoating; A homogeneous powder distribution across the entire scan plate surface is apparent, indicating uniformity of the powder application.



*Figure 6: Machine Modification / Setup*

**Single-Layer Experiment:** In the single-layer experiment, the surface roughness ( $R_a$ ) and energy density ( $E_l$ ) for Superpos1 and Superpos2 powders were analyzed. As shown in Figure 7, Superpos2 consistently exhibited larger  $R_a$  values across the entire spectrum of investigated  $E_l$  values. A co-linear trend between the powder-specific linear data regression suggested significant differences in the line roughness measurements between the two powders. To assess the significance of these differences, a one-way analysis of variance (ANOVA) was performed with a 95 % confidence interval and a significance level of 5 % ( $\alpha = 0.05$ ). The results yielded a p-value of  $0.996 \times 10^{-3}$  and an F-value of 18.77, leading to the rejection of the null hypothesis, which indicated that the  $R_a$  for Superpos1 and Superpos2 were not equivalent. This finding supports the conclusion that the PSD differences have a significant impact on the surface roughness. A general trend was identified in the data, where increased line roughness ( $R_a$ ) was observed with higher line energy density ( $E_l$ ), which is consistent with reports in the existing literature. A follow-up investigation is recommended to explore a wider range of process parameters to examine scan track consistency and the potential effects of powder PSD composition on initial humping or balling phenomena.

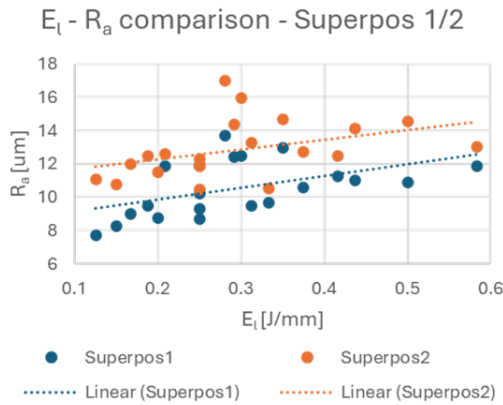


Figure 7: Setup Implementation

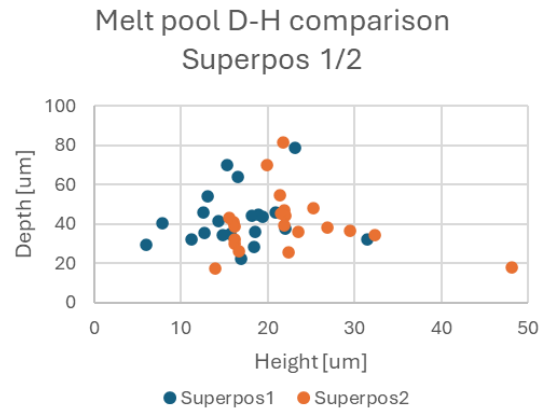


Figure 8: Melt Pool D-H Measurement Data

Regarding the melt pool geometry, no obvious differences were observed when comparing the melt pool depth (D) and height (H) individually across different energy densities. However, a more detailed analysis of the D/H ratios revealed distinct data separation between the two powders, as shown in Figure 8. Specifically, Superpos1, which consists of coarser powder, exhibited lower melt pool height (H) values for a given depth (D), while the finer Superpos2 powder showed increased melt pool heights for the corresponding depth measurements. This suggests that the D/H ratio is more sensitive to powder composition, warranting further investigation into its relationship with line energy density ( $E_l$ ) and other process parameters. When analyzing the D/H ratio over  $E_l$ , a clear data separation between Superpos1 and Superpos2 was evident. Superpos1 exhibited higher D/H values, indicating that the finer Superpos2 powder results in a decreased melt pool depth relative to height. A second ANOVA test was performed on the D/H data, and the results showed a p-value of 0.007 (p-value < 0.05), and an F-value of 8.16 leading to the rejection of the null hypothesis and confirming that the PSD significantly impacts the D/H ratio. Contour plotting of measured D/H ratios over the process parameters reveals increased regularity across the process parameter window with respect to the D/H metric. For the fine Superpos2 powder a primary dependency between D/H and the applied scan speed ( $v_s$ ) is apparent. The coarse Superpos1 powder, within the same parameter ranger for the power ( $P_i$ ) and scan speed ( $v_s$ ) exhibits an irregular trend behavior, whereas no continuous D/H trend dependency of the scan speed is observable. To verify detected trends and trend differences between the powder PSDs utilized additional replicas are required, furthermore intermediate factor levels, and parameter combinations, would increase the process parameter window resolution and hence support the identified trends. Concluding, the increase in line surface roughness ( $R_a$ ) and the decrease in D/H for the finer powder composition, indicates that a slight powder refinement significantly increases the balling tendencies, thus negatively affects the processability in PBF-LB/M

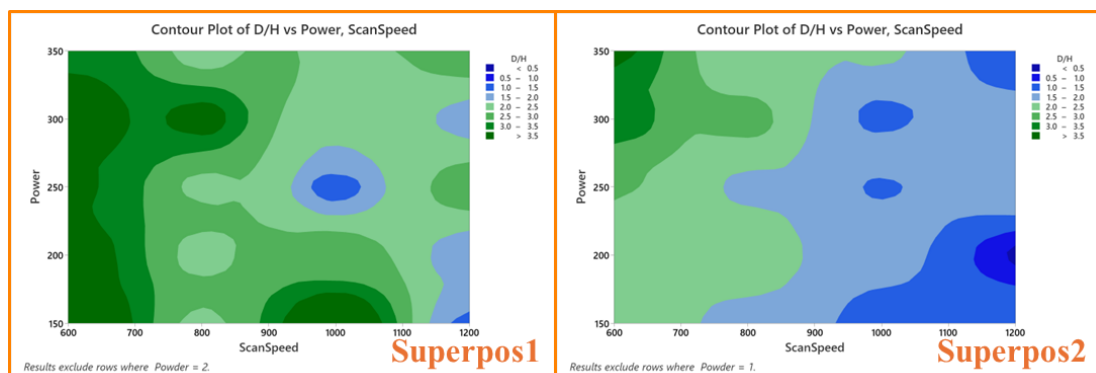


Figure 9: Single Layer Experiment Process Window

**Multi-Layer Experiment:** In the multi-layer experiment, several notable observations were made as depicted in Figure 10. Usage of the etchant Kallings No. 2 exhibited a color difference (blue – bronze) as shown in the accompanying images, whereas the specimen exhibits a blue tint for layers manufactured using the finer Superpos2 powder and a bronze tint for layers using the coarse Superpos1 powder. A transition zone between both specimen regions was identified for both specimens, which corresponds to the number of layers printed before the introduction of the other powder. This observation raises the question of whether thermal or heat flux conditions are responsible for the discoloration. It is hypothesized that the finer powder absorbs a greater fraction of the energy, leading to increased heat flux, higher temperatures, and possibly the evaporation of temperature responsive elements. Another explanation point for the visible discoloration is of chemical nature. Powder containing a greater volume fraction of fines could present a different chemical composition, alternatively evaporation due to differences in absorptivity as elaborated already potentially decreases the concentration of elements having lower evaporation temperatures. Adjusted in-depth investigations are necessary to characterize those explanations approaches in further detail to resolve the discoloration issue. Additionally, black dots, especially visible in the Superpos12 image, were identified as burn marks caused by the etchant accumulation in pore defects and surface cavities. The noticeable number of pore defects within the cutout of the manufactured specimens is determined to likely be caused by the unidirectional scan direction (in gas flow direction) chosen for the experiment to minimize the impact of in-process contamination of the specimen during manufacturing. An adjustment of the etching procedure could minimize the burn to provide even more comparable visual comparison, since etching is a manual/operator-dependent procedure. As depicted for Superpos21 where no black dot shaped and colored etching burns are visible, proper adjustment through increased/extended etching standardization/automation should be possible.

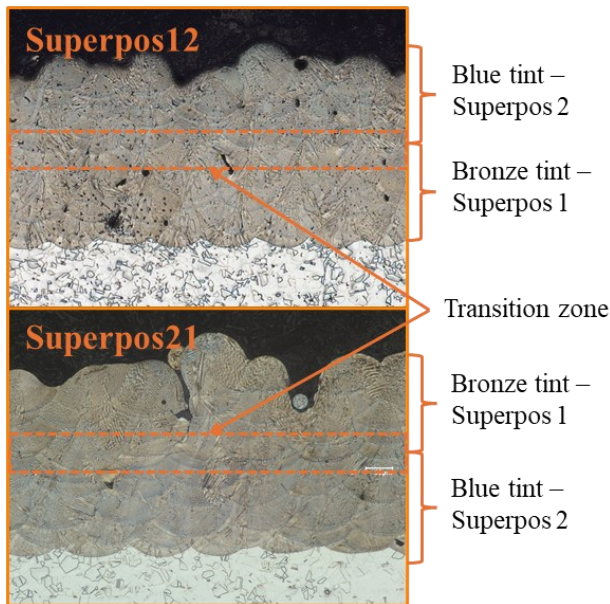


Figure 10: Visual Layer Differentiation

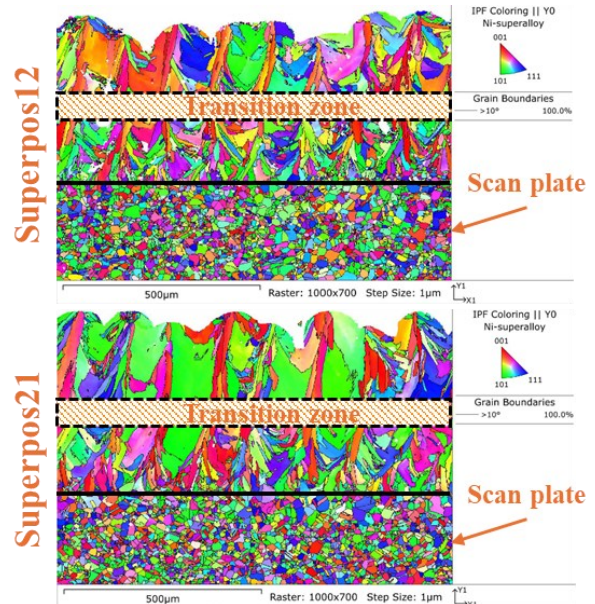


Figure 11: Micrograph Comparison

To statistically analyze the gathered HV0.1 hardness data through indentation, ANOVA testing was conducted using Minitab Statistical Software, with a one-way analysis of variance (ANOVA) at a 95% confidence interval and a significance level of 5% ( $\alpha = 0.05$ ). The null hypothesis, stating that the populations were the same, was rejected based on a p-value of  $0.681 \times 10^{-7}$  ( $\ll 0.05$ ) and an F-value of 88.36. This result supports the alternative hypothesis, indicating that the populations are not equivalent. The PSD difference between Superpos1 and Superpos2 causes a significant difference in the resulting hardness, with the finer Superpos2 powder exhibiting a hardness difference of more than 20 HV0.1, as depicted in Figure 12.

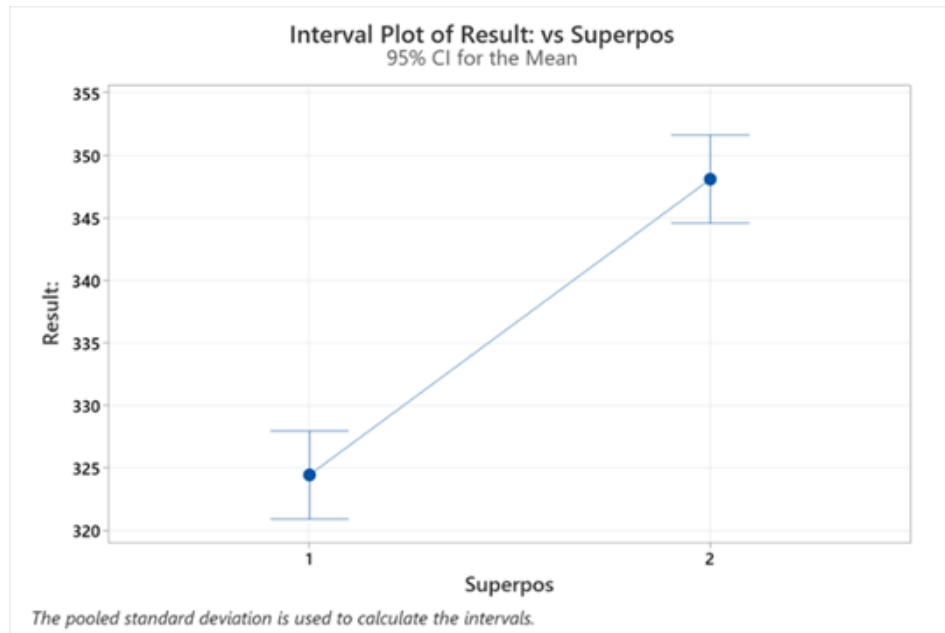


Figure 12: ANOVA Visualization

Sequence	Powder	Run	Avg. HV0.1	St.Dev.
Superpos12	1	1	325.9	15.1
Superpos12	2	1	340.1	3.8
Superpos12	1	2	320.4	6.8
Superpos12	2	2	343.8	9.1
Superpos21	1	1	329.8	6.8
Superpos21	2	1	354.0	10.9
Superpos21	1	2	321.6	12.4
Superpos21	2	2	354.4	9.1

Table 7: HV0.1 Measurement Data

Further ANOVAs were conducted to ensure that the HV0.1 values of Run 1 and Run 2 within the same sequence belonged to the same population. The results showed that for Superpos12, the p-value was 0.84 and the F-value was 0.04, indicating no significant difference in population. Similarly, for Superpos21, the p-value was 0.47 and the F-value was 0.498, suggesting the same conclusion. Considering all measurements presented in Table 7 and depicted in Figure 12, the average HV0.1 hardness value for the region of the specimen based on Superpos1 powder (coarser) was 324.4, while for Superpos2 (finer) powder, it was 348.1. Additional ANOVAs were conducted to examine whether the powder sequencing resulted in significant differences within the same specimen. For Superpos12, the p-value was much smaller than 0.05, with an F-value of 34.09, leading to the rejection of the equivalency hypothesis. Similarly, for Superpos21, the p-value was also much smaller than 0.05, with an F-value of 70.64, indicating that the populations are not equivalent. These results suggest that the HV0.1 hardness difference in Superpos21 is more pronounced than in Superpos12, likely due to heat flux and initial microstructural grain growth. To ensure consistency, similar ANOVAs were conducted for the indentation/hardness measurement runs to confirm statistical inference for the same powder in both specimens. The results showed that for Superpos12, the p-value was 0.84 and the F-value was 0.04, leading to the acceptance of the equivalency hypothesis. For Superpos21, the p-value was

0.47 and the F-value was 0.50, also supporting the equivalency hypothesis. One important factor contributing to the relatively high standard deviations observed was the measurement equipment calibration adjustment. Additionally, due to the thin layer of the same powder, a slight angular offset during indentation preparation may cause the last indents to shift into the transition zone or even into the area of the other powder. For future investigations, it is suggested to increase the number of supply chambers to ensure enough powder for an increased number of layers, which may help mitigate this issue. The consistently elevated HV0.1 hardness values for the finer powder, with the PSD composition being the only factor of variability in this experiment, suggest that a correlating change in microstructure might be present. Therefore, further investigation, especially with a focus on microstructural analysis, is recommended.

Preliminary microstructural analysis, as depicted in Figure 11, highlighted the need to adjust the experimental setup to perform more comprehensive microstructural analysis. In the Superpos12 specimen (top illustration), an obvious grain size difference between the powders was observed. Superpos2 (finer powder) above the transition zone depicted larger grains compared to Superpos1 (coarse powder) below the transition zone. In contrast, in the Superpos21 specimen (bottom illustration), Superpos1 (coarse powder) above the transition zone exhibited larger grains than Superpos2 (fine powder). This discrepancy suggests that grain sizes for Superpos1 do not match with the observations made for the Superpos12 specimen, while Superpos2 grain sizes are, on a qualitative basis, comparable to those seen in Superpos12. For Superpos21, unlike Superpos12, continuous grain growth through the transition zone was observed. This difference may be explained by the experimental setup, which involved applying only four powder layers of distinct PSD, subsequently scanned. During exposure, the laser penetrates and re-solidifies previous layers, leading to continuous grain growth that is not limited to layers of equivalent PSD. Thus, cross-influence between Superpos1 and Superpos2 powder could occur, preventing distinct grain growth. It is recommended to increase the number of powder layers for each powder type to ensure complete grain growth separation. However, as shown in previous investigations, finer powders exhibit a significantly higher absorptivity coefficient compared to coarser powders, which could result in different initial conditions for grain growth based on powder sequencing. A potential solution is to manufacture individual specimens consisting of only one powder composition, although this might compromise direct comparability due to slight differences in environmental factors and setup conditions, such as brush-scan plate alignment. One remaining challenge is understanding why HV0.1 hardness measurements for the same powder in both specimens were statistically equivalent despite being seemingly unaffected by the microstructure. A deeper chemical analysis is recommended to determine whether the consistent hardness difference is due to categorical differences in the chemistry of the powders. The finer powder particles may have a higher ratio of certain elements, and due to differences in absorptivity, these elements could evaporate differently depending on the powder particle size distribution. This could provide insights into the observed hardness variations.

## Conclusion

This study successfully validated the experimental setup for both single-layer and multi-layer experiments, yielding significant results regarding the effects of powder particle size distribution (PSD) on the geometry, surface roughness, hardness, and microstructure of parts produced using Laser Powder Bed Fusion (PBF-LB/M).

**Single-Layer Experiment:** Surface roughness ( $R_a$ ) analysis revealed that finer powder (Superpos2) exhibited significantly higher line surface roughness values, indicating increased balling tendency. This could be attributed to differences in energy absorption and melt pool geometry. The D/H ratio was identified as the only melt pool geometry metric showing differences for the investigated powder compositions. The finer powder resulted in an increased melt pool height, leading to a reduced D/H ratio. Furthermore, the process window for finer powder was wider and more stable, indicating improved process control and more consistent melt pool geometry. This highlights the importance of adjusting process parameters such as the laser powder ( $P_i$ ) and scan speed ( $v_s$ ) as the governing parameters for the line ( $E_l$ ) and volumetric ( $E_v$ ) energy density equations to accommodate powder bed location variations, ensuring consistent processability and part quality

across the entire powder bed/substrate plate. Future investigations should involve an extended factor level array of process parameters to determine stability boundaries through scan track continuity and explore the influence of a third PSD factor level.

**Multi-Layer Experiment:** In the multi-layer experiments, layer discoloration was observed to be independent of powder sequence, with finer powder (Superpos2) showing a blue discoloration and coarser powder (Superpos1) exhibiting a bronze color. Significant differences in hardness (HV0.1) were observed, with the finer powder (Superpos2) exhibiting an at least 6.8 % higher hardness (HV0.1 = 348.1) compared to the coarser powder (HV0.1 = 324.4). These hardness differences were independent of the powder sequence, indicating the need for further investigation into the microstructure to better understand the root causes of these differences. Additional replicas are necessary to ensure the consistency and repeatability of these results, and further exploration of a third PSD factor level is needed to determine if these trends are continuous or regular.

The results highlight the need for software tools applicable at the shop floor level to compensate for “Lot-to-Lot” PSD variations through appropriate powder blending or modification. Additionally, further investigation is required to determine whether the detected differences in mechanical properties are fundamentally caused by microstructural differences due to PSD alone, or by chemical variations, or a combination of both. Literature often suggests that chemistry is particle size-dependent and thus may be the driving factor behind the observed differences in mechanical properties, melt pool geometry, and surface roughness. However, this hypothesis needs to be validated, as such studies have not yet been conducted in realistic application scenarios, such as the one presented in this research. In conclusion, finer powders exhibited a more stable process and significantly higher hardness values. Further research into the microstructure, chemical composition, and underlying physical mechanisms is necessary to better understand and validate the observed phenomena.

### **Acknowledgements**

The research presented was performed at The University of Texas at El Paso within the W.M. Keck Center for 3D Innovation. The constant support of Jorge Mireles and Ryan B. Wicker are highly. This material is based on research sponsored by Air Force Research Laboratory under agreement number FA8650-20-2-5700. The U.S. Government is authorized to reproduce and distribute reprints for Governmental purposes notwithstanding any copyright notation thereon. The views and conclusions contained herein are those of the authors and should not be interpreted as necessarily representing official policies or endorsements, either expressed or implied, of Air Force Research Laboratory or the U.S. Government.

### **Data and Availability**

The measurement and analysis raw data for presented investigation results and technical drawings of the designed components are available and can be provided upon request, as well as equipment setup settings. Additionally, the RStudio and Python scripts used for data analysis are also available. For further inquiries or to request access to the materials, please contact via email at: nicolas.pielczyk@googlemail.com.

### **References**

- [1] B. Blakey-Milner *et al.*, "Metal additive manufacturing in aerospace: A review," *Materials & Design*, vol. 209, 2021
- [2] A. Boretti, "A techno-economic perspective on 3D printing for aerospace propulsion," *Journal of Manufacturing Processes*, vol. 109, 2024

- [3] J. H. Warner, S. P. Ringer, and G. Proust, "Strategies for metallic powder reuse in powder bed fusion: A review," *Journal of Manufacturing Processes*, vol. 110, 2024
- [4] F. J. Alamos *et al.*, "Effect of powder reuse on mechanical properties of Ti-6Al-4V produced through selective laser melting," *International Journal of Refractory Metals and Hard Materials*, vol. 91, 2020
- [5] "sdm15-038," <https://nimbusvault.net/publications/koala/inimpact/papers/sdm15-038.pdf>
- [6] R. Harkin, H. Wu, S. Nikam, J. Quinn, and S. McFadden, "Reuse of Grade 23 Ti6Al4V Powder during the Laser-Based Powder Bed Fusion Process," *Metals*, vol. 10, no. 12, 2020
- [7] V. V. Popov *et al.*, "Powder Bed Fusion Additive Manufacturing Using Critical Raw Materials: A Review," *Materials*, vol. 14, no. 4, 2021
- [8] S. Ziri, A. Hor, and C. Mabru, "Combined effect of powder properties and process parameters on the density of 316L stainless steel obtained by laser powder bed fusion," (in En;en), *Int J Adv Manuf Technol*, vol. 120, 9-10, 2022
- [9] K. Gruber, I. Smolina, and W. Stopyra, "Assessing metal powder quality for additive manufacturing using diffuse light spectroscopy," *Powder Technology*, vol. 434, 2024
- [10] C. Pleass and S. Jothi, "Influence of powder characteristics and additive manufacturing process parameters on the microstructure and mechanical behaviour of Inconel 625 fabricated by Selective Laser Melting," *Additive Manufacturing*, vol. 24, 2018
- [11] M. Xue, X. Chen, X. Ji, X. Xie, Q. Chao, and G. Fan, "Effect of Particle Size Distribution on the Printing Quality and Tensile Properties of Ti-6Al-4V Alloy Produced by LPBF Process," *Metals*, vol. 13, no. 3, 2023
- [12] Z. K. Snow, "17825," [https://etda.libraries.psu.edu/files/final\\_submissions/17825](https://etda.libraries.psu.edu/files/final_submissions/17825)
- [13] F. Chu *et al.*, "Influence of powder size on defect generation in laser powder bed fusion of AlSi10Mg alloy," *Journal of Manufacturing Processes*, vol. 94, 2023
- [14] J. Zhang and Y.-G. Jung, Eds., *Additive Manufacturing: Materials, Processes, Quantifications and Applications*: Elsevier, 2018.
- [15] R. Lachmayer, T. Ehlers, and R. B. Lippert, "Basics," in *Design for Additive Manufacturing*, R. Lachmayer, T. Ehlers, and R. B. Lippert, Eds., 1st ed., Berlin, Heidelberg: Springer Berlin Heidelberg, Imprint: Springer, 2024
- [16] J. Berez, E. Dushaj, E. Jost, C. Saldaña, and K. Fu, "Measurement of focal plane error in laser powder bed fusion machines," *Additive Manufacturing Letters*, vol. 9, 2024
- [17] K. Takaku, S. Suzuki, T.-T. Ikeshoji, and H. Kyogoku, "Assessing powder processability and melting behavior in powder-bed fusion additive manufacturing," *Materials & Design*, vol. 240, 2024
- [18] S. Pal *et al.*, "The effects of locations on the build tray on the quality of specimens in powder bed additive manufacturing," (in En;en), *Int J Adv Manuf Technol*, vol. 112, 3-4, 2021
- [19] S. E. Brika and V. Brailovski, "Influence of Powder Particle Morphology on the Static and Fatigue Properties of Laser Powder Bed-Fused Ti-6Al-4V Components," *JMMP*, vol. 4, no. 4, 2020
- [20] S. A. Farzadfar, M. J. Murtagh, and N. Venugopal, "Impact of IN718 bimodal powder size distribution on the performance and productivity of laser powder bed fusion additive manufacturing process," *Powder Technology*, vol. 375, 2020
- [21] Z. Fang, B. Patterson, and M. Turner, "Influence of particle size distribution and coarsening," *Acta metall. mater.*, vol. 40, 1992
- [22] M. Salandre, S. Garabedian, G. Gaillard, T. Williamson, and T. Joffre, "Development of a New Tooling Steel (L40) for Laser Powder Bed Fusion: Influence of Particle Size Distribution and Powder Atomization on Mechanical Performance," *Adv Eng Mater*, vol. 23, no. 9, 2021
- [23] M. Horn *et al.*, "Multi-Material Additive Manufacturing – Recycling of binary Metal Powder Mixtures by Screening," *Procedia CIRP*, vol. 93, 2020
- [24] ASM International, *Additive manufacturing processes*. Materials Park, Ohio: ASM International, 2020
- [25] P. Moghimian *et al.*, "Metal powders in additive manufacturing: A review on reusability and recyclability of common titanium, nickel and aluminum alloys," *Additive Manufacturing*, vol. 43, 2021